Evaluation of cold wire addition on pitting corrosion behavior of SAW duplex stainless steel welds

Neice F. Santos[a], Ronaldo C. Júnior[b], Paulo J. Modenesi[c], Vanessa F. C. Lins[d], Emerson Giovani Rabello[e], Luiza Esteves[f]

Abstract

Duplex stainless steels (DSS) have been placed as an excellent alternative for applications where high corrosion resistance and high mechanical strength are required. Otherwise, when DSS are welded, the experienced thermal history may severely impair their performance, especially local pitting corrosion resistance and toughness. The aim of this work was to evaluate the influence of three distinct cold wire feeding rate (CW) on the pitting corrosion behavior of DSS bead-on-plate welds performed over lean duplex stainless steel UNS S32304 plates using submerged arc welding (SAW) with cold wire addition. Cyclic potentiodynamic polarization (CPP) was carried out in transversal weld sections using 1 M NaCl solution. All pitting corrosion spots were located on the heat affected zone (HAZ) and the pitting potentials have reduced in comparison with base metal due to higher ferrite fractions and the presence of chromium nitrides in this region. Among the three test conditions, pitting corrosion potential has decreased with the increase of CW, due to higher ferrite content in the HAZ when CW was raised.

Keywords: cold wire addition, duplex stainless steel, pitting corrosion, SAW

Introduction

Duplex stainless steels (DSS) have an attractive combination of its mechanical properties, corrosion resistance and good weldability (ANTONY et al., 2008; ZHANG et al., 2016) due their dual-phase microstructure containing a ferrite/austenite (α/γ) ratio close to 1:1 (ANTONY et al., 2008; LIOU; HSIEH; TSAI, 2002; ZHANG et al., 2016). These steels are used in wide range of applications, such as oil and gas, chemical and petrochemical industries, nuclear industries, pulp and paper, desalination, etc. (RUIZ et al., 2016; SARLAK; ATAPOUR; ESMAILZADEH, 2015; ZHANG et al., 2016). In order to maintain a localized corrosion resistance equivalent to austenitic stainless steels and reduce the cost compared to conventional DSS, lean duplex stainless steels (LDSS) have been developed, which have

[a] Engenheira Química – CDTN/CNEN
[b] Mestre, Engenheiro Químico - ESAB
[c] Doutor, Engenheiro Metalúrgico – UFMG
[d] Doutora, Engenheira Química – UFMG
[e] Doutor, Engenheiro Metalúrgico – CDTN/CNEN
[f] Doutora, Química Industrial – CDTN/CNEN

reduced molybdenum and nickel contents, the most common is the UNS S32304 (BRYTAN; NIAGAJ; REIMAN, 2016; KARLSSON et al., 2010; WESTIN, 2010).

However, after DSS have been welded, the experienced thermal history may severely impair their performance, especially local pitting corrosion resistance and toughness (JIANG et al., 2013). DSS presents a fully ferritic microstructure at high temperatures, thus rapid welding cooling rates will result in excessive ferritization of the heat-affected zone (HAZ) and weld metal (CHEHUAN et al., 2014; KIM et al., 2014; WESTIN, 2010) and in addition, there is a formation of nitride precipitates (Cr_2N, CrN) (BRYTAN; NIAGAJ; REIMAN, 2016; KARLSSON, 2012; MOHAMMED et al., 2017; SATHIRACHINDA et al., 2010).

The addition of a cold wire represents an interesting alternative to raise the deposition rate without adding extra heat (MOHAMMADIJOO et al., 2017; XIANG et al., 2016). Although several studies have been reported about cold wire addition in SAW for carbon steel grades (MOHAMMADIJOO et al., 2017; RAMAKRISHNAN; MUTHUPANDI, 2013; XIANG et al., 2016), there is a scarce information for DSS.

In this work, the effect of three distinct CW on the pitting corrosion behavior of DSS bead-on-plate welds performed over LDSS UNS S32304 plates using SAW ICE^{TM} was investigated by the cyclic potentiodynamic polarization (CPP) in 1 M NaCl solution at room temperature.

Materials and methods

The LDSS plate was supplied by Aperam South America (Brazil) in hot rolled and annealed conditions. Bead on plate welds were carried out using UNS S32304 plates with 12 mm nominal thickness, 300 mm long and 300 mm wide. As filler metal, AWS A5.9 ER2209 solid wires were used, 2.50 mm diameter, and a basic non alloying flux designed for stainless steel welding application, were was supplied by ESAB Indústria e Comércio LTDA. Chemical composition of the plate and welding wire are shown in Table 1.

As a welding system, SAW ICE^{TM} was used head powered as a 1000 A AC/DC power source. In this system, three wires are fed simultaneously, the two external hot wires are connected to the power source while the central one (cold wire) is not. The ratio between the cold and hot wires feed speed can be set in the equipment and is termed as CW along this paper.

Welding trials were performed with one heat input level of 2.2 kJ/mm, varying a cold/hot wires feed ratio of 0, 50 and 100%. These percentages correspond to the ratio of the feed rate of the cold wire to the hot wire. By the equipment construction concept, the cold wire feed speed is parameterized as a ratio percentage of the energized wire feed speed. For all the trials, the welding speed, current and voltage were maintained constant at 55 cm/min, 550 A and 37 V, respectively. The welding was performed in DC+ polarity and the stick out was maintained constant at 25 mm. In order to identify the samples studied, the following nomenclature was adopted, as presented in Table 2.
Microstructural characterization and electrochemical tests were performed transversally to the welding direction. To assess the macro and microstructure, the samples were mechanically polished, etched with Behara II, and then examined by an optical microscope (OM). The immersion time in the Behara II solution was about 5 s for OM.

The corrosion resistance evaluation of the welded LDSS were studied using cyclic potentiodynamic polarization (CPP). The test surface area exposed to corrosion test was approximately 400 mm^2, covering all the weld metal, HAZ and base metal (BM). The samples were embedded in epoxy resin, wet ground to 600 grit, and the electrical connections were made by welding a copper wire to the test piece. The samples were wet ground to 600 grit SiC abrasive papers, and cleaned with distilled water and ethanol, dried with hot air. In order to avoid crevices, the edge samples embedded in epoxy resin were sealed by epoxy resin (Araldite) at least 12 h before testing and were stored in a desiccator. The areas of the samples were determined using the software Image J.

The CPP testing was performed using an Autolab PGSTAT 100 potentiostat. A conventional three-electrode arrangement was used for the measurements with welded specimens as the working electrodes, a platinum mesh as the counter electrode and silver/silver chloride electrode (Ag/AgCl, 3M KCl) as the reference electrode. The open circuit potential was monitored during 1 hour until its stabilization. The CPP curves were collected by scanning in the anodic direction at a scan rate of 1 mV/s from 20 $mV_{Ag/AgCl}$ below the corrosion potential (Ecorr). Scanning was reversed when the current reached 3 mA/cm^2. All the electrochemical measurements were repeated at least three times to ensure the reproducibility. The tests were carried out in 1 mol/L NaCl aqueous solution at room temperature. After testing, pit morphology was observed by using SEM analysis.

Results and discussion

The microstructure of the FZ/HAZ/BM transition region is shown in Figure 1. It is possible to observe that the HAZ has a significant ferritization, while it observes higher fractions of austenite in the FZ and BM. DSS is sensitive to ferritization, due to its metallurgy and the fast cooling rate during welding, which causes the unbalance of its microstructure (ARTURO et al., 2015; JANG et al., 2011). The higher amount of austenite in the FZ is due to the fact that the greater amount of Ni in the addition metal than in the base metal, in order to avoid similar ferritization behavior in the welded metal.

CPP tests were conducted in an aqueous solution of 1 mol/L NaCl at room temperature. The cyclic potentiodynamic polarization curves are shown in Figure 2. The electrochemical parameters such as Ecorr, passivation current density (Ipass) and Epit for each test condition are listed in Table 3 (values are an average of at least three measures). Another method to evaluate pitting corrosion resistance is the difference between Epit and Ecorr as: ΔE = Epit - Ecorr (Table 3) (A. IGUAL MUÑOZ et al., 2004).

With an increase of CW, the Epit and the current density of repassivation decrease. But it is noteworthy that the density values of the passivation current are in the same order of magnitude for both test conditions. The order of magnitude of 10^{-6} indicates a protective passive layer. Welded joints showed a defined similar corrosion behavior.

The optical micrographs of welded joints after the CPP tests are shown in Figure 3. It is observed that the HAZ of the welded joints proved to be the region most susceptible to localized corrosion. Tan et al. (2011) observed that welded joints exhibited impaired pitting corrosion resistance, and pitting occurred preferentially on ferrite grains of the HAZ near the melt line (TAN et al., 2011). Chen et al. (2012) found that the resistance to pitting corrosion

of HAZ in AILD UNS S32304 decreased with increasing cooling rate and pitting occurred in the ferritic phase. In addition, the pitting corrosion resistance of DSS in HAZ can be influenced by chromium nitrides (Cr_2N) and inclusions (CHEN et al., 2012).

Pitting potential decreased with an increase of cold wire feeding rate (CW). This can be explained by the higher ferrite content in the HAZ when CW raised, whereas, the ferrite presents less PREN in relation to austenite in DSS (ZHANG et al., 2012). The precipitation of secondary phases generates poor regions in Cr, Mo and N with reduced PREN, also leading to the loss of resistance to pitting (LO; SHEK; LAI, 2009; MAGNABOSCO; ALONSO-FALLEIROS, 2005).

Conclusions

Joints of LDSS welded in different conditions were tested in chloride environment. Based on the results, it is possible to conclude:

- The HAZ had a significant ferritization, while it was observed higher fractions of autenite in the FZ and BM.
- With an increase of CW, the Epit and the current density of repassivation decrease.
- The HAZ of the welded joints proved to be the region most susceptible to localized corrosion. In addition, the pitting corrosion resistance of DSS in HAZ can be influenced by chromium nitrides (Cr_2N) and inclusions.
- Pitting corrosion potential decreased with an increase of cold wire feeding rate (CW). This can be explained by the higher ferrite content in the HAZ when CW raised, whereas the ferrite presents less PREN in relation to austenite in DSS. The precipitation of secondary phases generates poor regions in Cr, Mo and N with reduced PREN, also leading to the loss of resistance to pitting

Acknowledgments

The authors are grateful to the Brazilian government agencies (CNPq, CNEN, CAPES and FAPEMIG) for the financial support for this research and Centro de Desenvolvimento da Tecnologia Nuclear (CDTN/CNEN) for the technical support.

Referências bibliográficas

A. IGUAL MUÑOZ et al. Corrosion Behavior of Austenitic and Duplex Stainless Steels in Lithium Bromide. **Corrosion**, v. 60, n. 10, p. 982–995, 2004.

ANTONY, P. J. et al. Corrosion of 2205 duplex stainless steel weldment in chloride medium containing sulfate-reducing bacteria. **Metallurgical and Materials Transactions A: Physical Metallurgy and Materials Science**, v. 39, n. 11, p. 2689–2697, 2008.

ARTURO, G. R. M. et al. Electrochemical Characterization of AISI 2205 Duplex Stainless Steel Welded Joints with Electromagnetic Interaction. **Procedia Materials Science**, v. 8, p. 950–958, 2015.

BRYTAN, Z.; NIAGAJ, J.; REIMAN. Corrosion studies using potentiodynamic and EIS electrochemical techniques of welded lean duplex stainless steel UNS S82441. **Applied Surface Science**, v. 388, p. 160–168, 2016.

CHEHUAN, T. et al. Influence of multipass pulsed gas metal arc welding on corrosion behaviour of a duplex stainless steel. **Corrosion Science**, v. 86, p. 268–274, 2014.

CHEN, L. et al. Influence of cooling rate on microstructure evolution and pitting corrosion

resistance in the simulated heat-affected zone of 2304 duplex stainless steels. **Corrosion Science**, v. 58, p. 168–174, 2012.
JANG, S.-H. et al. Effect of Shielding Gas Composition on Phase Transformation and Mechanism of Pitting Corrosion of Hyper Duplex Stainless Steel Welds. **Materials Transactions**, v. 52, n. 6, p. 1228–1236, 2011.
JIANG, Y. et al. Influence of Cr eq / Ni eq on pitting corrosion resistance and mechanical properties of UNS S32304 duplex stainless steel welded joints. **Corrosion Science**, v. 70, p. 252–259, 2013.
KARLSSON, L. et al. Effects of Alloying Concepts on Ferrite Morphology and Toughness of Lean Duplex Stainless Steel Weld Metals. **Welding in the World**, v. 54, n. 11–12, p. R350–R359, 2010.
KARLSSON, L. Welding Duplex Stainless Steels - A Review Of Current Recommendations. **Welding in the World**, v. 56, n. 5–6, p. 65–76, 2012.
KIM, H. J. et al. Investigation of the sensitization and intergranular corrosion of tube-to-tubesheet welds of hyper duplex stainless steel using an electrochemical reactivation method. **Corrosion Science**, v. 87, p. 60–70, 2014.
LIOU, H. Y.; HSIEH, R. I.; TSAI, W. T. Microstructure and pitting corrosion in simulated heat-affected zones of duplex stainless steels. **Materials Chemistry and Physics**, v. 74, n. 1, p. 33–42, 2002.
LO, K. H.; SHEK, C. H.; LAI, J. K. L. Recent developments in stainless steels. **Materials Science and Engineering: R: Reports**, v. 65, n. 4–6, p. 39–104, maio 2009.
MAGNABOSCO, R.; ALONSO-FALLEIROS, N. Pit morphology and its relation to microstructure of 850 degrees C aged duplex stainless steel. **Corrosion**, v. 61, n. February, p. 130–136, 2005.
MOHAMMADIJOO, M. et al. Evaluation of cold wire addition effect on heat input and productivity of tandem submerged arc welding for low-carbon microalloyed steels. **International Journal of Advanced Manufacturing Technology**, v. 92, n. 1–4, p. 817–829, 2017.
MOHAMMED, G. et al. Effects of Heat Input on Microstructure, Corrosion and Mechanical Characteristics of Welded Austenitic and Duplex Stainless Steels: A Review. **Metals**, v. 7, n. 2, p. 39, 2017.
RAMAKRISHNAN, M.; MUTHUPANDI, V. Application of submerged arc welding technology with cold wire addition for drum shell long seam butt welds of pressure vessel components. **International Journal of Advanced Manufacturing Technology**, v. 65, n. 5–8, p. 945–956, 2013.
RUIZ, A. et al. Microstructural and ultrasonic characterization of 2101 lean duplex stainless steel welded joint. **Applied Acoustics**, v. 117, p. 8, 2016.
SARLAK, H.; ATAPOUR, M.; ESMAILZADEH, M. Corrosion behavior of friction stir welded lean duplex stainless steel. **Materials and Design**, v. 66, n. PA, p. 209–216, 2015.
SATHIRACHINDA, N. et al. Study of nobility of chromium nitrides in isothermally aged duplex stainless steels by using SKPFM and SEM/EDS. **Corrosion Science**, v. 52, p. 179–186, 2010.
TAN, H. et al. Annealing temperature effect on the pitting corrosion resistance of plasma arc welded joints of duplex stainless steel UNS S32304 in 1.0M NaCl. **Corrosion Science**, v. 53, n. 6, p. 2191–2200, 2011.
WESTIN, E. **Microstructure and properties of welds in the lean duplex stainless steel LDX 2101**. [s.l.] Royal Institute of Technology, Stockholm, Sweden, 2010.
XIANG, T. et al. Effects of filling status of cold wire on the welding process stability in twin-

arc integrated cold wire hybrid welding. **International Journal of Advanced Manufacturing Technology**, v. 83, n. 9–12, p. 1583–1593, 2016.
ZHANG, Z. et al. Microstructural evolution and pitting resistance of annealed lean duplex stainless steel UNS S32304. **Nuclear Engineering and Design**, v. 243, p. 56–62, 2012.
ZHANG, Z. et al. Investigation on microstructure evolution and properties of duplex stainless steel joint multi-pass welded by using different methods. **Materials and Design**, v. 109, p. 670–685, 2016.

Tables

Table 1 - Chemical composition of plate (UNS S32304 LDSS) and wire (AWS A5.9 ER2209).

Material	Concentration of alloying element (wt.%)										
	C	**Mn**	**Si**	**P**	**S**	**Cr**	**Ni**	**Mo**	**Cu**	**Nb**	**N**
Plate	0.011	1.46	0.36	0.023	0.0003	22.28	4.01	0.28	0.44	0.009	0.12
Wire	0.012	1.70	0.47	0.020	0.0010	22.80	8.70	3.10	0.10	0.009	0.17

Table 2: Identification of samples

Samples	Heat input (kJ/mm)	ICE (%)	Identification
Welded Joint	2.2	0	2.2 – 0
		50	2.2 – 50
		100	2.2 - 100
Bse Metal	-	-	BM

Table 3 - Electrochemical parameters of DSS welds

Samples	E_{corr} ($mV_{Ag/AgCl}$)	I_{pass} ($\mu A/cm^2$)	E_{pit} ($mV_{Ag/AgCl}$)	E_{prot} ($mV_{Ag/AgCl}$)	ΔE (E_{pit}-E_{corr}) ($mV_{Ag/AgCl}$)
2.2 - 0	-156.0 ± 11.3	0.9 ± 0.3	480.5 ± 0.8	-	636.5 ± 12.2
2.2 – 50	-150.5 ±4.9	0.5 ± 0.2	462.6 ± 14.0	-	613.1± 9.0
2.2 - 100	-154.3 ± 13.5	0.4± 0.2	435.6 ± 20.2	-	589.9 ± 20.1
MB	-162.3 ± 5.5	1.3 ± 0.2	557.9 ± 3.8	-93.4 ± 28.1	720.3 ± 8.5

Figures

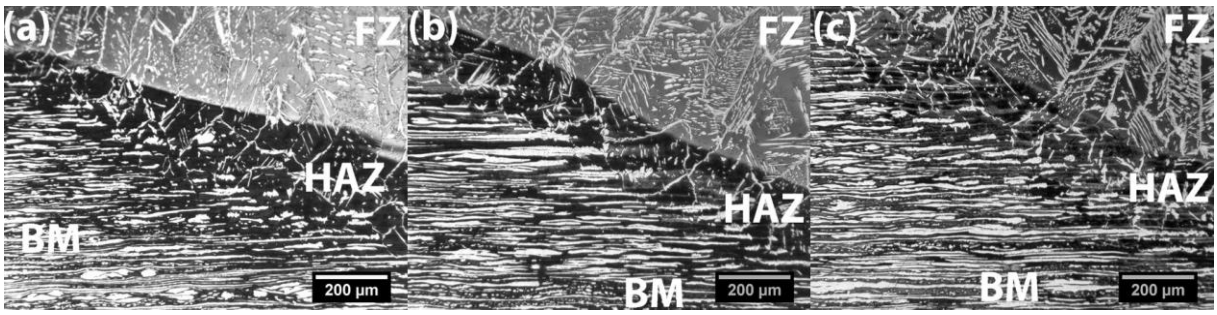

Figure 1 - Optical microscopy of the transition region (ZF/HAZ/BM) in the (a) 2.2-0, (b) 2.2-50 and (c) 2.2-100 welding conditions

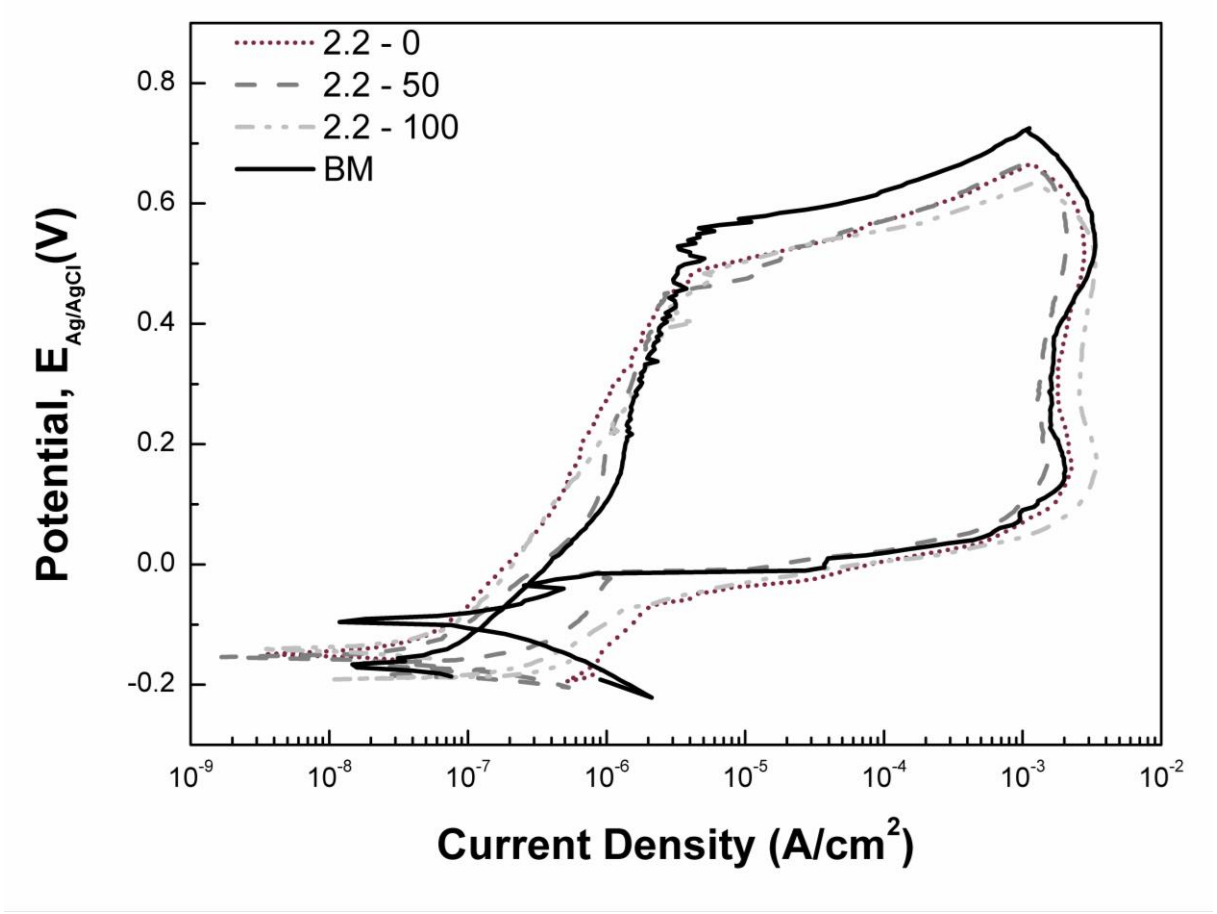

Figure 2 - Cyclic potentiodynamic polarization curves for welded joints in 1 mol/L NaCl at room temperature

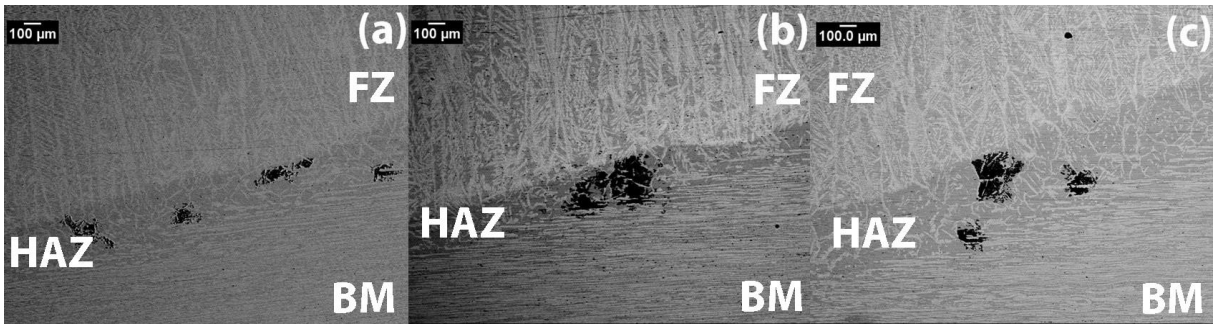

Figure 3 - SEM after CPP showing pits in the HAZ.